On the Closed Form Mechanistic Modeling of Milling: Specific Cutting Energy, Torque, and Power

A.E. Bayoumi, G. Yücesan, and D.V. Hutton

Specific energy in metal cutting, defined as the energy expended in removing a unit volume of workpiece material, is formulated and determined using a previously developed closed form mechanistic force model for milling operations. Cutting power is computed from the cutting torque, cutting force, kinematics of the cutter, and the volumetric material removal rate. Closed form expressions for specific cutting energy were formulated and found to be functions of the process parameters: pressure and friction for both rake and flank surfaces and chip flow angle at the rake face of the tool. Friction is found to play a very important role in cutting torque and power. Experiments were carried out to determine the effects of feedrate, cutting speed, workpiece material, and flank wear land width on specific cutting energy. It was found that the specific cutting energy increases with a decrease in the chip thickness and with an increase in flank wear land.

Keywords
milling, modeling, specific cutting energy, torque, power, tool wear

1. Introduction

MACHINABILITY of materials is often measured by the total energy used in removing a unit volume of work material, which is called specific cutting energy (SPCE). In most material removal processes, SPCE can be used as an efficiency indicator of the machining process. Specific cutting energy includes the energy expended in the primary and secondary deformation zones, interfacial friction activities at the tool/workpiece interfaces, and energy needed for the generation of new surfaces. This energy is transferred from the cutting tool through the cutter rake and flank surfaces to the chip, workpiece, and heat as the cutting process takes place. In general, specific cutting energy is a function of particular workpiece material properties and cutting conditions such as feed, speed, and tool geometry. For a particular set of cutting conditions and cutting tool/workpiece combination, this energy is found to be inversely proportional to the chip thickness.[1,2] It was also reported by these investigators that specific cutting energy decreases as the chip thickness increases and that cutting speed has minimal effect on the energy at higher cutting speeds. It has been suggested by Boothroyd[2] that the increase in specific cutting energy with a decrease in the chip thickness could be attributed to the increased ratio of the plowing force or size effect as the chip thickness decreases. The plowing force results from the roundness of the cutting edges and the deformation of the tool material under the high stresses acting on the tool edges. For a freshly ground high-speed cutting tool, this radius is reported to vary from 0.005 to 0.03 mm.[2] In practice, for nonzero tool nose radius, there is a limit on the undeformed chip thickness below which the cutting action becomes a rubbing or extrusion process rather than a typical chip formation. If the chip thick-

A.E. Bayoumi, G. Yücesan, and **D.V. Hutton,** Department of Mechanical and Materials Engineering, Washington State University, Pullman, WA 99164-2920.

Nomenclature

F	Cutting force
F_f	Friction force
F_y	Cutting in the y-direction for sharp tool
f_t	Feedrate
K_f	Rake friction parameter
K_{feff}	Effective average friction parameter
K_{ff}	Flank friction parameter
K_n	Rake pressure parameter
K_{neff}	Effective average pressure parameter
K_{nf}	Flank pressure parameter
L_f	Width of the flank wear land
$\vec{n}$	A unit vector normal to the cutter surface
P	Power
R	Radius of a point on the cutting edge
R_a	Axial engagement
R_d	Radial engagement
$SPCE$	Specific cutting energy
$SPCE_{eff}$	Average specific cutting energy
T	Torque
$\vec{T_c}$	A unit vector in the chip movement direction
t_c	Chip thickness
v	Volumetric removal rate
v_{ave}	Average volumetric removal rate
v_c	Cutting speed
v_y	Feed speed
α	Position angle with respect to the lowest cutting point
α_1	Lower integration limit
α_2	Upper integration limit
α_{en}	Radial engagement angle
α_r	Rake angle of the cutter in x-y plane
α_{ra}	Axial engagement angle of a cutting point
θ	Rotation angle for a single fluted cutter
θ_c	Chip flow angle
θ_{ceff}	Effective average chip flow angle
θ_h	Cutter helixangle

ness is smaller than such a limit, plowing becomes the dominant component of the cutting forces. This, in turn, increases the specific cutting energy, because this force does not contribute to the material removal.

There are several areas where specific cutting energy can be used for metal cutting operations. In using SPCE as a machinability index, higher specific cutting energy indicates lower machinability and vice versa. Because it depends on the cutting conditions, favorable cutting conditions can be selected by minimizing the SPCE index. Specific cutting energy can also be used to analyze and accurately generate CNC part programs, thus minimizing the trial and error process. Similarly, specific cutting energy can be used as the basis for a control algorithm for both off-line and on-line adaptive control environment.

The objective of this investigation was to model specific cutting energy, torque, and power for milling operations in a closed form mechanistic approach. The previously developed mechanistic milling force model was used as a basis to determine the cutting torque and power. The variations of pressure, friction, and chip flow direction at the tool/workpiece interface with the rotation angle of the tool were included in the energy model. The effects of the feedrate, width of flank wear, and spindle speed on SPCE were investigated in cutting 11L17 free-machining steel. The remainder of this article presents the torque formulation, specific cutting energy analysis, and an experimental verification of the method.

2. Development of Torque Equations

The mechanistic milling force model that was used as a basis for the development of the specific cutting energy has been published elsewhere.[3,4] The model was originally developed by integrating the pressure and friction loads at the tool/workpiece surface interface to obtain the overall cutting forces exerted on the cutting edge. The assumptions made in the development of the mechanistic force model (no built-up edge formation, chatter-free operation, and rigid tool) also apply to this study. To eliminate the effects of runout offset, a single fluted helical end mill cutter was used. For cases with runout, the methodology is general, and runout effects can be considered easily by using the modified chip thickness relationships given by Kline et al.[5] As has been presented in the development of the general closed form mechanistic cutting force model, the normal force acting on the cutter rake surface is written[4] as:

$$d\vec{F}_n = -K_n(\alpha,\theta)\,\mathbf{A}\,(\theta)\,\vec{n}(\alpha)\,dA \qquad [1]$$

where $K_n(\alpha,\theta)$ is the pressure parameter; α is the position angle of a point; θ is the rotation angle of the cutter; and dA is the undeformed chip cross section area which is computed as:

$$dA = t_c(\alpha,\theta)dS \qquad [2]$$

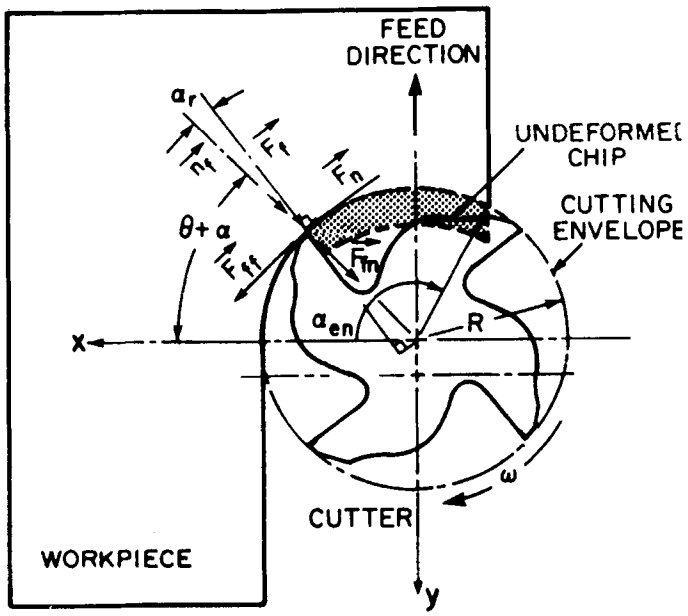

Fig. 1 *x-y* plane projection of the cutter forces.

with

$$t_c = f_t \sin(\alpha + \theta)$$

and

$$dS = \frac{Rd\alpha}{\sin\theta_h}$$

where t_c is the chip thickness; f_t is the feed rate; R is the cutter radius; θ_h is the helix angle; and $\mathbf{A}(\theta)$* is a transformation matrix that rotates the cutter and it can be expressed as:

$$\mathbf{A}(\theta) = \begin{pmatrix} \cos\theta & -\sin\theta & 0 \\ \sin\theta & \cos\theta & 0 \\ 0 & 0 & 1 \end{pmatrix} \qquad [3]$$

Similarly, the frictional force component is

$$d\vec{F}_f = K_n(\alpha,\theta)\,K_f(\alpha,\theta)\,\mathbf{A}\,(\theta)\,\vec{T}_c\,(\alpha)\,dA \qquad [4]$$

where $K_f(\alpha,\theta)$ is the friction parameter at the cutting surface/chip interface, and $\vec{T}_c\,(\alpha)$ and $\vec{n}(\alpha)$ are the unit chip movement direction vector and unit normal vector, respectively, and are given as:

*In actual cutting, the cutter rotates in an opposite direction to the position angle, α. In this investigation, the cutter flute wraps counterclockwise around the cutter and the cutter rotates in the clockwise direction. Thus, θ accepts negative values.

$$\vec{n}(\alpha) = A \sin(\alpha - \alpha_r)\,\vec{i} - A \cos(\alpha - \alpha_r)\,\vec{j} + B\,\vec{k}$$

$$\vec{T_c}(\alpha) = \{\, C \sin\alpha - D \cos(\alpha - \alpha_r) \,\}\,\vec{i} - \{\, C \cos\alpha + D \sin(\alpha - \alpha_r) \,\}\,\vec{j} + E\,\vec{k} \quad [5]$$

where

$$A = \frac{\cos\theta_h}{\sin\theta_{tk}}$$

$$B = \frac{\cos\alpha_r}{\sin\theta_{tk}} \sin\theta_h$$

$$C = \sin\theta_h(\cot\theta_{tc}\cos\theta_c - \sin\theta_c)$$

$$D = \frac{\cos\theta_c}{\sin\theta_{tk}}$$

$$E = \cos\theta_h(\sin\theta_c - \cos\theta_c\cot\theta_{tk})$$

$$\theta_{tk} = \cos^{-1}[\sin\alpha_r \sin\theta_h] \quad [6]$$

Integrating Eq 1 and 4 and using the appropriate integration limits, the force relationships can be obtained.[4]

The torque acting on the cutter is divided into two components—the rake and the flank torque— that result from the distributed pressure and friction loading acting on the rake and flank surfaces, respectively. Only x and y components of the normal and friction forces have an effect on the cutting torque, as is shown in Fig. 1. The torque generated by the pressure loading acting on an infinitesimal rake surface element can be obtained as:

$$dT_{zrn} = R\cos\alpha_r\sqrt{(dF_{nx}^2 + dF_{ny}^2)} \quad [7]$$

where

$$dF_{nx} = \frac{-Rf_tK_n(\alpha,\theta)}{\sin\theta_h} A \sin(\alpha+\theta)\sin(\alpha+\theta-\alpha_r)d\alpha$$

and

$$dF_{ny} = \frac{Rf_tK_n(\alpha,\theta)}{\sin\theta_h} A \sin(\alpha+\theta)\cos(\alpha+\theta-\alpha_r)d\alpha$$

where α_r is the cutter rake angle in the $x-y$ plane. The torque generated by the pressure loading acting on an infinitesimal rake surface segment can thus be obtained as:

$$dT_{zrn} = A\frac{R^2f_tK_n(\alpha,\theta)}{\sin\theta_h}\cos\alpha_r \sin(\alpha+\theta)d\alpha \quad [8]$$

Similarly, the torque generated by the friction loading acting on an infinitesimal rake surface segment can be written as:

$$dT_{zrf} = R\sin\alpha_r\sqrt{(dF_{fx}^2 + dF_{fy}^2)} \quad [9]$$

where

$$dF_{fx} = \frac{Rf_tK_n(\alpha,\theta)\,K_f(\alpha,\theta)}{\sin\theta_h}\sin(\alpha+\theta)\{\, C\sin(\alpha+\theta) - D\cos(\alpha+\theta-\alpha_r)\,\}\,d\alpha$$

$$dF_{fy} = \frac{Rf_tK_n(\alpha,\theta)\,K_f(\alpha,\theta)}{\sin\theta_h}\sin(\alpha+\theta)\{-C\cos(\alpha+\theta) - D\sin(\alpha+\theta-\alpha_r)\,\}\,d\alpha$$

Substituting dF_{fx} and dF_{fy} into Eq 9 yields:

$$dT_{zrf} = R^2\frac{f_tK_n(\alpha,\theta)\,K_f(\alpha,\theta)}{\sin\theta_h}\sin\alpha_r\sin(\alpha+\theta)\{C^2 + D^2 - 2CD\sin\alpha_r\}^{1/2}d\alpha \quad [10]$$

In analyzing the forces acting on the cutting edge, one finds that the flank normal force, acting in the radial direction, does not generate any torque. The torque generated by flank friction force acting on the infinitesimal flank surface element can be computed as:

$$dT_{zff} = K_{nf}(\alpha,\theta)K_{ff}(\alpha,\theta)Rl_f\cot\theta_hR\,d\alpha \quad [11]$$

The total torque acting on an infinitesimal cutter flute element can then be obtained by adding the rake and flank torque components as:

$$dT_z = dT_{zrn} + dT_{zrf} + dT_{zff} \quad [12]$$

The total torque acting on a single flute for a certain engagement can then be obtained by integrating Eq 12 over the engaged length of the cutter flute. The cutter torque is obtained as a function of the rotation angle as:

$$T_z(\alpha) = \int_{\alpha_1(\theta)}^{\alpha_2(\theta)} dT_z \quad [13]$$

If moving effective values of process parameters as presented by the authors elsewhere[6] are used, Eq 13 can be integrated to obtain a closed form equation for the cutter torque as:

$$T_z(\theta) = \frac{R^2K_{neff}(\theta)f_t}{\sin\theta_h}\{-\cos(\alpha+\theta)[\cos\alpha_rA + K_{feff}(\theta)\sin\alpha_r(C^2+D^2-2CD\sin\alpha_r)] + K_{nf}K_{ff}R^2l_f\cot\theta_h\alpha\,\}\Big|_{\alpha_1(\theta)}^{\alpha_2(\theta)} \quad [14]$$

Where $\alpha_1(\theta)$ and $\alpha_2(\theta)$ are the integration limits, which are functions of the tool rotation angle and axial and radial depths of cut (engagements). Integration limits can be obtained as a function of the tool rotation angle as follows:

$$\alpha_1(\theta) = \begin{cases} 0 & \text{for} \quad 0 \geq \theta \geq -\alpha_{en} \\ \alpha_{en} + \theta & \text{for} \quad -\alpha_{en} \geq \theta \geq -(\alpha_{en} + \alpha_{ra}) \\ 0 & \text{otherwise} \end{cases} \quad [15]$$

and

$$\alpha_2(\theta) = \begin{cases} -\theta & \text{for} \quad 0 \geq \theta \geq -\alpha_{ra} \\ \alpha_{ra} & \text{for} \quad -\alpha_{ra} \geq \theta \geq -(\alpha_{ra} + \alpha_{en}) \\ 0 & \text{otherwise} \end{cases} \quad [16]$$

where α_{en} is the radial engagement angle, and α_{ra} is the axial engagement angle computed as:

$$\alpha_{ra} = \frac{R_a}{R \cot \theta_h}$$

$$\alpha_{en} = \cos^{-1}\left(\frac{R - R_d}{R}\right) \quad [17]$$

The total torque acting on a multiple-flute cutter can be obtained by summing the torque generated by each flute as:

$$T_z(\theta) = \sum_{i=1}^{N_f} T_z(\theta_i)$$

where N_f is the number of flutes, and θ_i is the rotation angle for the i^{th} flute measured from the initial engagement of the i^{th} flute. θ_i can be expressed as:

$$\theta_i = \theta + \frac{2\pi(i-1)}{N_f}$$

Integration limits for the i^{th} flute are obtained by replacing θ in Eq 15 and 16 by θ_i. Average cutter torque can be obtained by integrating the cutter torque over the engagement period and dividing by the engagement period as:

$$T_{zave} = \frac{1}{(\alpha_{en} + \alpha_{ra})} \int_0^{\alpha_{en}+\alpha_{ra}} T_z(\theta) d\theta$$

or

$$T_{ave} = \frac{\alpha_{ra}}{(\alpha_{en} + \alpha_{ra})} \frac{R^2 K_{neff} f_d}{\sin \theta_h} (1 - \cos \alpha_{en}) \left[A \cos \alpha_r + K_{feff} \sin \alpha_r (C^2 + D^2 - 2CD, \sin \alpha_r)^{1/2} \right] + K_{nf} K_{ff} R l_f \cot \theta_h R \, \alpha_{en} \quad [18]$$

The total average torque for a multiple-fluted cutter can then be calculated as:

$$T_{ave}(N_f) = \frac{N_f(\alpha_{en} + \alpha_{ra})}{2\pi} T_{ave} \quad [19]$$

3. Formulation of Specific Cutting Energy

Having the cutter torque sufficiently formulated, the specific cutting energy can be determined mathematically by dividing the expended power by the volumetric material removal rate. The volumetric removal rate is a function of chip thickness and cutting speed. In milling, chip thickness changes with the cutter rotation angle. Therefore, the specific cutting energy changes as the cutter rotates. The power consumed on an infinitesimal cutter surface segment can be formulated as:

$$dP = dT \cdot \omega + F_y \cdot v_y \quad [20]$$

where dP is the power expended to machine an infinitesimal volume of the workpiece; ω is the angular speed of the spindle; F_y is the cutting force in the Y-direction for sharp cutters; and v_y is the feedrate. As the feedrate is small relative to spindle speed, power consumption in the feed direction is negligible compared to the other component.

The specific cutting energy at a point located on the cutting edge at any instant can be written as:

$$SPCE = \frac{dP}{dv} \quad [21]$$

where dv is the volumetric removal rate defined on an infinitesimal cutting surface given by

$$dv = t_c(\alpha + \theta) R(\alpha) \, \omega \frac{R(\alpha) d\alpha}{\sin \theta_h} \quad [22]$$

Substituting Eq 12 and 22 into Eq 21, the specific cutting energy at any point located on the cutter edge can be found as:

$$SPCE(\alpha,\theta) = \frac{K_n(\alpha,\theta) \left\{ F + GK_f(\alpha,\theta) \right\}}{\sin \theta_h} + \frac{k_{nf}(\alpha,\theta) k_{ff}(\alpha,\theta) \cos \theta_h l_f}{t_c(\alpha + \theta)} \quad [23]$$

where

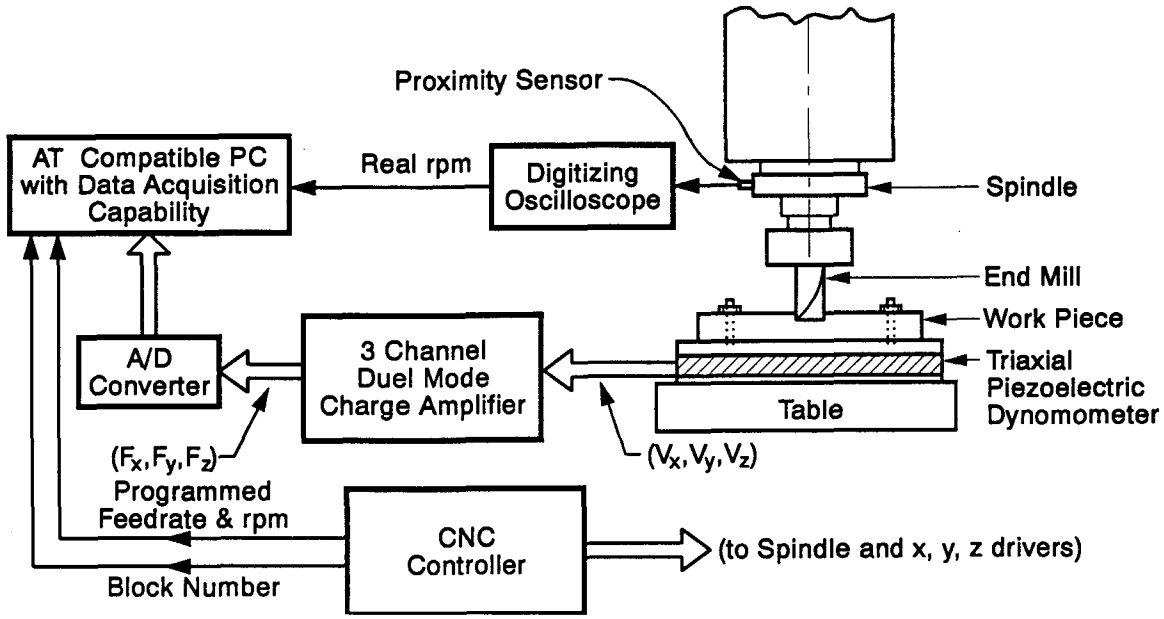

Fig. 2 Schematic of the experimental setup.

$$F = A \cos \alpha_r$$

$$G = \sin \alpha_r \{ C^2 + D^2 - 2CD \sin \alpha_r \}^{1/2}$$

and l_f is the flank wear land.

It can be seen from Eq 23 that the specific cutting energy is a function of the cutter geometry and the process parameters. These process parameters for particular cutting conditions are, in turn, functions of the location angle α and the tool rotation angle θ. As the tool rotates, the parametric behavior at any point follows a periodic time history. Therefore, an overall performance of a particular cutting operation based on the instantaneous specific cutting energy may not be feasible. To define an overall performance measure for a particular cut, an effective value of the specific cutting energy needs to be determined. Using the chip thickness as a weighting factor, this effective value of specific cutting energy is determined as:

$$SPCE_{eff} = \frac{\int_0^{\alpha_{en}} SPCE(\alpha = 0, \theta) \sin(\theta) d\theta}{\int_0^{\alpha_{en}} \sin(\theta) d\theta} \quad [24]$$

or

$$SPCE_{eff} = \frac{K_{neff}\left(F + GK_{feff}\right)}{\sin \theta_h} + \frac{k_{nfeff}\, k_{ffeff} \cos \theta_h l_f}{f_t(1 - \cos \alpha_{en})} \quad [25]$$

where

$$K_{neff} = \frac{\int_0^{\alpha_{en}} K_n(\alpha = 0, \theta) \sin\theta d\theta}{\int_0^{\alpha_{en}} \sin\theta d\theta} \quad [26]$$

The other parameters, K_{feff}, K_{nfeff}, K_{ffeff}, and θ_{ceff} are expressed and determined in a similar manner to that of K_{neff} (Eq 26).

4. Experimental Work

With the formulation of the torque and specific cutting energy established, some experimental work is required to verify the approach and to show the capabilities of the concepts. A 2-1/2 axis Bridgeport Series I CNC milling machine is used in the experiments. A Kistler three-component measuring platform is used to measure the cutting forces. The analog force signals are amplified and passed to an A/D converter for sampling and storage via a microcomputer. To minimize measurement noise, the amplifier settings were selected depending on the expected range of the cutting force components. A digitizing oscilloscope is coupled with a magnetic pickup coil to precisely determine the spindle speed. The magnetic pickup coil is attached to a housing surrounding the spindle shaft that has a hole drilled in it. As the shaft rotates, the hole acts as a discontinuity and disrupts the magnetic field of the magnetic pickup coil and generates an electrical signal. This signal is fed into the digitizing oscilloscope to determine the spindle rotational frequency. Figure 2 is a schematic of the experimental setup.

Two series of tests were carried out using sharp and worn cutters. Tests using sharp cutters were conducted to determine the rake pressure, friction, and chip flow angle parameters.[4]

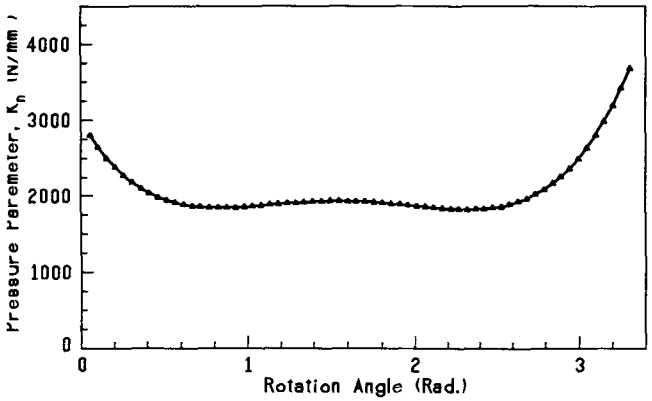

Fig. 3 Pressure parameter induced in cutting 11L17 free-machining steel using a single-fluted sharp milling cutter. Cutter diameter, 16 mm; R_a, 3.8 mm; f_d, 0.056 mm; N, 700 rpm.

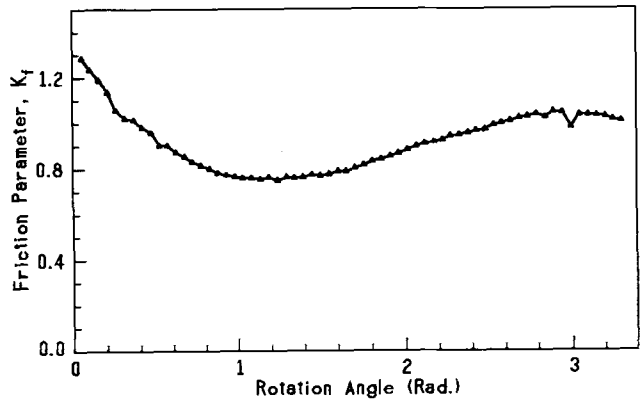

Fig. 4 Friction parameter induced in cutting 11L17 free-machining steel using a single-fluted sharp milling cutter. Cutter diameter, 16 mm; R_a, 3.8 mm; f_d, 0.056 mm; N, 700 rpm.

Similarly, tests using worn cutters were performed to obtain the flank parameters. For these tests, flank wear was artificially generated on HSS end milling cutters using a cylindrical grinding machine. The artificial flank wear land width was measured using a tool microscope with a magnification of 100× that is equipped with a digital readout.

The range of feed rate was established such that the minimum feedrate is influenced by the rubbing mechanism at the cutting edge.[6] The upper limit values are dictated by the initiation of chatter and excessive vibration of the machine tool. The maximum feedrate value is observed to decrease with increased amount of artificially imposed flank wear land. The minimum value is found to increase with an increase in the flank wear land value.[7] In other words, the range is narrowed with increasing wear.

5. Presentation and Discussion of Results

It has been assumed throughout this investigation that rake pressure and friction are not significantly affected by the wear development on the flank surface as the cutting progresses. Supporting evidence for such an assumption is reported by several researchers, see for example Koren et al.[8] and Ko et al.[9] Therefore, the forces acting on the flank surfaces (as predicted by the model) were obtained by subtracting the total force acting on the sharp cutter from the total forces obtained in the tests using a worn cutter under the same testing conditions. The flank pressure and friction parameters were computed from the flank forces obtained in this manner using a mechanistic tool wear model.[7] During testing, the cutting conditions were selected such that no chatter or excessive vibration were present.

Rake pressure parameter is closely related to the chip thickness value.[7] As the chip thickness becomes smaller, this parameter increases. It has been found that rake friction parameter and chip flow directions are inversely related, and this is in agreement with earlier findings of Zorev[1] and Shaw.[10] As the friction decreases, chip flow angle increases and vice versa. In Fig. 3 to 5, rake pressure, friction, and chip flow angle parameters are shown as functions of tool rotation

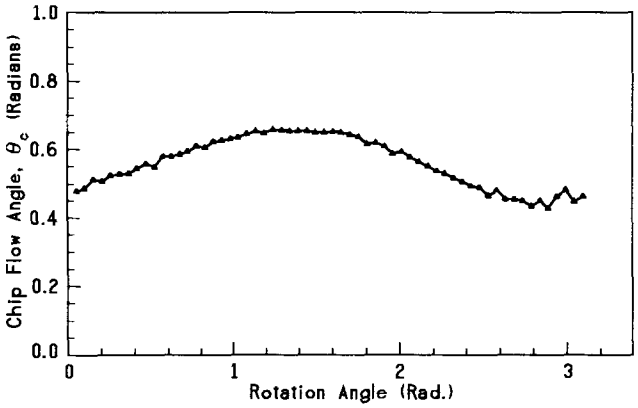

Fig. 5 Chip flow angle at the chip/tool face interface in cutting 11L17 free-machining steel using a single-fluted sharp milling cutter. Cutter diameter, 16 mm; R_a, 3.8 mm; f_d, 0.056 mm; N, 700 rpm.

angle in cutting 11L17 free-machining steel. Average flank pressure and friction are observed to vary slightly with feedrate. Flank pressure and friction change linearly with flank wear land width and cutting speed. Details of this study were presented by the authors elsewhere.[11] Relationships between the flank parameter and width of the flank wear land were given[7] as:

$$K_{nf} = \begin{cases} 1884 l_f - 181.5 \text{ for } = l_f > 0.095 \text{ mm} \\ 0 \text{ for } = l_f < 0.095 \text{ mm} \end{cases} \quad [27]$$

$$K_{ff} = -1035 l_f + 0.96$$

Moreover, flank friction was found to be independent of the tool rotation angle and its value was found to be in close agreement with the average rake friction parameter.

Figure 6 shows the cutter torque as a function of the rotation angle for a sharp milling cutter and for different levels of flank

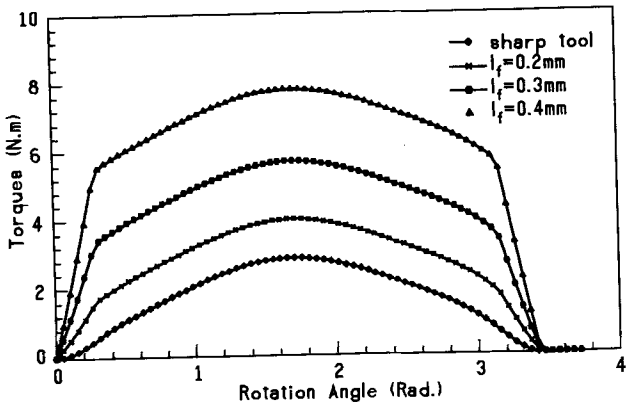

Fig. 6 Induced torque in cutting 11L17 free-machining steel at different levels of flank wear land development.

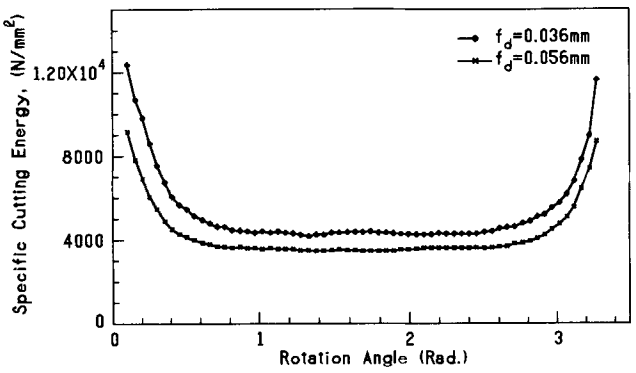

Fig. 8 Effect of feedrate on the specific cutting energy in cutting 11L17 free-machining steel. Cutter diameter, 16 mm; R_a, 5 mm; N, 700 rpm.

wear land. It can be seen that cutting torque increases with an increase in flank wear. Expended cutting power increases proportionally with cutting torque. This torque behavior as the rotation angle increases has shown that the torque increases with an increase in chip thickness, and the maximum torque occurs around maximum value of the undeformed chip thickness.

In analyzing the formulation of the specific cutting energy, it was shown that SPCE is a function of the process parameters and tool geometry. Figure 7 shows the behavior of the specific cutting energy for a sharp milling cutter and for different flank wear land levels. It can be seen that the specific cutting energy increases with an increase in flank wear. For a flank wear land value of 0.4 mm, the amount of energy to remove a unit volume of material doubles in comparison to that of 0.1 mm wear land. In general, specific cutting energy follows the same trend as the pressure parameter. The flank term in the specific cutting energy expression is inversely proportional to the undeformed chip thickness. However, because the flank pressure becomes zero around small chip thickness values, it counterbalances the chip thickness, which appears in the denominator, as the chip thickness becomes zero. This limit value of the specific cutting energy cannot be shown experimentally because the measurement noise and unmodeled effects become dominant in the measured force signals, especially during tool entry and exit

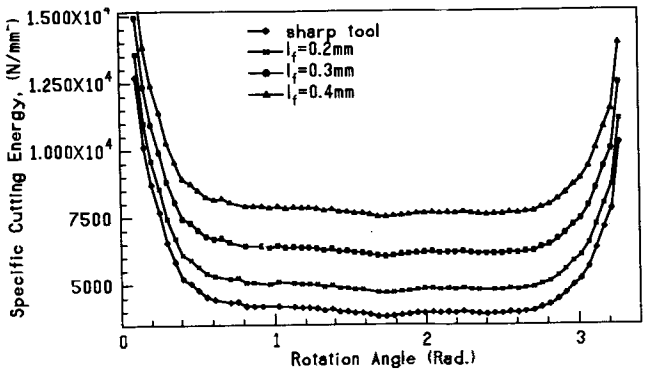

Fig. 7 Effect of flank wear land on the specific cutting energy in cutting.

from the workpiece. For very small flank wear lands, there is no indication of change in the cutting forces. Accordingly and as is expected, it was observed that there is no significant change in the specific cutting energy.

Figure 8 shows the specific cutting energy for a slotting cut as a function of the rotation angle in cutting 11L17 free-machining steel at different feedrates. As the feedrate decreases, the specific energy increases. These results are anticipated because the rake pressure and friction increase, and the volumetric material removal rate decreases with a decrease in feedrate with no significant change in the flank pressure and friction parameters. This is in good agreement with the plowing force, or size effect mechanism, previously suggested by Boothroyd.[2] In computing the data for Fig. 8, the following linear relationships that were obtained by the authors elsewhere[4,11] for the flank pressure and friction parameters as functions of the feedrate were

$$k_{nf}(f_d) = -1266f_d + 240$$
$$k_{ff}(f_d) = 11.13f_d + 0.287 \quad [28]$$

Figure 9 shows the effect of cutting speed on the specific cutting energy. Similar linear relationships for the average flank pressure and friction parameters as functions of cutting speed were used in computing values of Fig. 9:

$$k_{nf} = 0.320v_c - 20.75$$
$$k_{ff} = -0.239v_c + 0.97 \quad [29]$$

The specific cutting energy is relatively independent of cutting speed when cutting with sharp milling cutters at medium to high cutting speeds. However, when machining the same material under the same cutting conditions using worn milling cutters, specific cutting energy was found to increase. This may be attributed to the strain-rate hardening of the very small layer of the machined workpiece surface under the pressure and friction loading around the flank interface surfaces.[12]

Figure 10 shows the specific cutting energy for three different work materials (11L17 free-machining steel, 2024 aluminum, and 360 free-machining brass) under similar testing conditions except cutting speeds. It can be seen that the specific

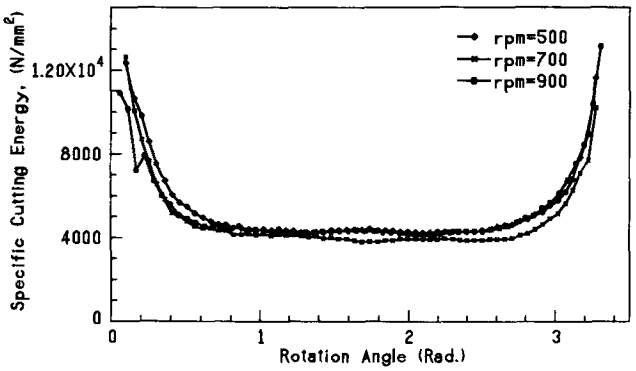

Fig. 9 Effect of cutting speed on the specific cutting energy in cutting 11L17 free-machining steel. Cutter diameter, 16 mm; R_a, 5 mm; N, 700 rpm.

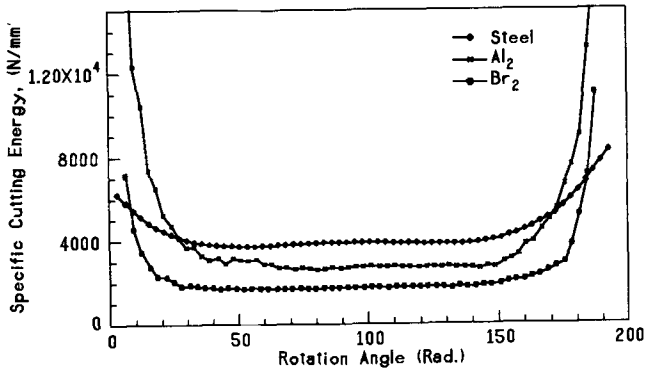

Fig. 10 Specific cutting energy in cutting free-machining 11L17 steel, 2024 aluminum, and a free-machining brass.

cutting energy for these three different materials follows similar trends. At higher chip thickness values, the steel work material exhibits the highest specific cutting energy. However, around small chip thickness values, the specific cutting energy of 2024 aluminum material exceeds that for the steel workpiece. Therefore, machinability of 2024 aluminum, at small chip thickness values, is worse than that for 11L17 steel. Therefore, faster tool nose rounding rates may be expected when machining aluminum workpieces than that for steel. Also, the specific cutting energy along with the chip thickness can be used as an indicator of tool edge condition.

The results depicted in Fig. 6 and 7 indicate a strong potential for monitoring cutting tool wear via on-line measurement of torque or specific cutting energy. The data depicted in these figures correspond to a particular set of cutting conditions and, as can be observed from Eq 14 and 23, the curves will shift up or down for other engagements and feedrates. Nevertheless, an intelligent monitoring system can be conceived for batch-produced components in which the part program and synchronized spindle drive current measurements are used to establish baseline sharp cutter levels for each machining operation during production of the first few components. During continuing production, torque or SPCE level for each part program block would be compared to the baseline data for indication of tool edge condition. The major advantage of such a system is that no force measurement is required, and there is thus no need for intrusive instrumentation. In fact, for most modern automated machine tools, no additional instrumentation would be required because the majority of current technology machine tool controllers provide both spindle speed and spindle motor current levels. Together with known characteristics of the spindle drive system, this provides sufficient information to compute the required parameters.

6. Conclusions

The following conclusions were drawn from this investigation. Specific cutting energy can be obtained using a mechanistic force model. This energy is the function of mechanistic process parameters, chip thickness, and the width of flank wear land. Flank wear land and chip thickness are the two most important factors affecting specific cutting energy. Specific cutting energy increases with an increase in the flank wear land width and a decrease in the undeformed chip thickness, which is in agreement with the findings of previous research. Unlike cutting force and cutting torque, specific cutting energy is a scalar quantity that is a simple function that provides the amount of energy expended in removing a unit volume of workpiece material. Therefore, specific cutting energy can be used as a simplistic performance measure for machining operations. Specific cutting energy may also be used as an indicator to estimate the width of the flank wear land. The measure of specific cutting energy during the tool entry and exit may be used as an indicator for tool nose rounding and/or wear rate.

References

1. N.N. Zorev, *Metal Cutting Mechanics*, C.M. Shaw, Ed., translated by H.S.H. Massey, Pergamon Press, 1966
2. G. Boothroyd, *Fundamentals of Metal Machining and Machine Tools*, Scripta Book Co., 1975
3. G. Yucesan, A.E. Bayoumi, and L.A. Kendall, An Analytic Cutting Force Model for Milling, *Trans. NAMRC*, Vol XVIII, 1990, p 137-145
4. G. Yucesan, A.E. Bayoumi, and L.A. Kendall, An Analytic Closed-Form Mechanistic Cutting Force Model for Milling Operations: A Theory and Methodology, *JEI-ASME*, 1994, to be published
5. W.A. Kline, R.E. DeVor, and J.R. Lindberg, The Prediction of Cutting Forces in End Milling with Application to Cornering Cuts, *Int. J. Mach. Tool Des. Res.*, Vol 22 (No. 1), 1982, p 7-22
6. *Machining Data Handbook*, Vol 1, 3rd ed., Metcut Research Associates Inc., 1980
7. T.M. Teitenberg, A.E. Bayoumi, and G. Yucesan, Tool Wear Modeling Through an Analytic Mechanistic Model of Milling Processes, *Int. J. Wear*, Vol 154, 1991, p 287-304
8. Y. Koren, K. Danai, A. Ulsoy, and T. Ko, Monitoring Tool Wear Through Force Measurement, *NAMRC XV*, May 1987, p 463-468
9. T. Ko and Y. Koren, Cutting Force Model for Tool Wear Estimation, *NAMRC XVII*, May 1989, p 166-169
10. C.M. Shaw, *Metal Cutting Principles*, Vol 3, Oxford Series on Advanced Manufacturing, Clarendon Press, 1984
11. G. Yucesan, A.E. Bayoumi, and L.A. Kendall, An Analytic Closed-Form Cutting Force Model: A Case Study of Helical Milling Operation, *JEI-ASME*, 1994, to be published
12. D.A. Rigney and J.P. Hirth, Plastic Deformation and Sliding Friction of Metals, *Wear*, Vol 53, 1979, p 345-370